

Electromagnetic design of the KATRIN large-volume air coil system

Ferenc Glück¹, Guido Drexlin¹, Benjamin Leiber¹, Susanne Mertens^{1,2}, Alexander Osipowicz³, Jan Reich¹ and Nancy Wandkowsky¹

¹ KCETA, Karlsruhe Institute of Technology, Karlsruhe, Germany

²Lawrence Berkeley National Laboratory, Berkeley, USA

³University of Applied Sciences, Fulda, Germany

E-mail: ferenc.glueck@kit.edu

Abstract.

The KATRIN experiment is designed to determine the absolute neutrino mass scale with a sensitivity of 200 meV (90 % CL) by measuring the electron energy spectrum close to the endpoint of molecular tritium β decay. Electrons from a high-intensity gaseous tritium source are guided by a strong magnetic field of a few T to the analyzing plane of the main spectrometer where an integral energy analysis takes place in a low field region ($B < 0.5$ mT). An essential design feature to obtain adiabatic electron transport through this spectrometer is a large volume air coil system surrounding the vessel. The system has two key tasks: to adjust and fine-tune the magnetic guiding field (Low Field Correction System), as well as to compensate the distorting effects of the earth magnetic field (Earth Field Compensation System). In this paper we outline the key electromagnetic design issues for this very large air coil system, which allows for well-defined electron transmission and optimized background reduction in the KATRIN main spectrometer.

1. Introduction

Experimental information about the neutrino masses and lepton mixing is important both for particle physics and cosmology. The observation of flavor oscillations of atmospheric, solar, reactor and accelerator neutrinos has provided convincing evidence for lepton mixing and non-zero neutrino masses. However, neutrino oscillation studies only allow to access the mass splittings of various neutrino mass eigenstates, but yield no information on the absolute neutrino mass scale.

Cosmological observations [1] and neutrinoless double beta decay experiments [2] provide access to the absolute neutrino mass scale, but are rather model-dependent. On the other hand, a direct and model-independent way to measure the effective electron neutrino mass is possible by high-precision β -spectroscopy of nuclear β -decays close to the endpoint. The β -emitter with the best decay characteristics ($t_{1/2} = 12.3$ y and endpoint energy $E_0 = 18.6$ keV) is tritium [3, 4].

The Karlsruhe Tritium Neutrino (KATRIN) experiment [5] is designed to determine the absolute neutrino mass scale with a sensitivity of 200 meV by a precise measurement of the electron energy spectrum close to the endpoint E_0 of molecular tritium. In the 70 m long setup (see Fig. 1), electrons are guided from the source to the detector by magnetic fields in the range of a few T, which are created by many superconducting coils. The main spectrometer of the MAC-E filter type is on high negative potential (around -18.6 kV) and acts as an electrostatic filter for the integral energy spectrum measurement. In this filter type, only electrons with enough kinetic energy are able to be transmitted through the spectrometer to be counted at the detector. Inside the main spectrometer, we need a small magnetic field (below 0.5 mT), to convert most of the transversal energy of the β -decay electrons into longitudinal energy by the inverse magnetic mirror effect. To fine-tune this magnetic field for the purposes of the precise energy filtering and to compensate the disturbing effect of the earth magnetic field, a large volume (about 3000 m³) air coil system has been designed and built.

The main purpose of this paper is to discuss the most important electromagnetic design features of this coil system. The technical design of the system and results of corresponding magnetic field measurements will be presented in a second publication [6].

The plan of this paper is the following. In Sec. 2 we give a short overview of the main KATRIN components, and point out the key design requirements that are relevant for the successful air coil operation. In Sec. 3 we discuss the adiabatic longitudinal and transmission energy of electrons and also define the notion of analyzing point and the transmission condition. Then we explain why and how the transmission condition in the main spectrometer should be fulfilled. Sec. 4 contains a description of the most important requirements about the magnetic field inside the main spectrometer, and the specific role of the air coil system to fulfill these requirements is explained. Sec. 5 is devoted to a detailed explanation of the axisymmetric part of the air coil system (LFCS), and in Sec. 6 the non-axisymmetric earth field compensating part (EMCS) is described. In Appendix A we give a short overview about the magnetic and electric field simulation methods that have been used for the air coil design. Finally, in Appendix B we present a multiobjective mathematical optimization method that is useful to compute various LFCS coil current configurations.

2. The KATRIN experiment

In this section we give a short overview of the main components of the KATRIN experiment, emphasizing those details that are important for the electromagnetic design issues of the KATRIN air coil system. For more details about the KATRIN experiment we refer to Refs. [3, 4, 5, 7, 8].

The 70 m long KATRIN setup (see Fig. 1) contains the following main components:

WGTS

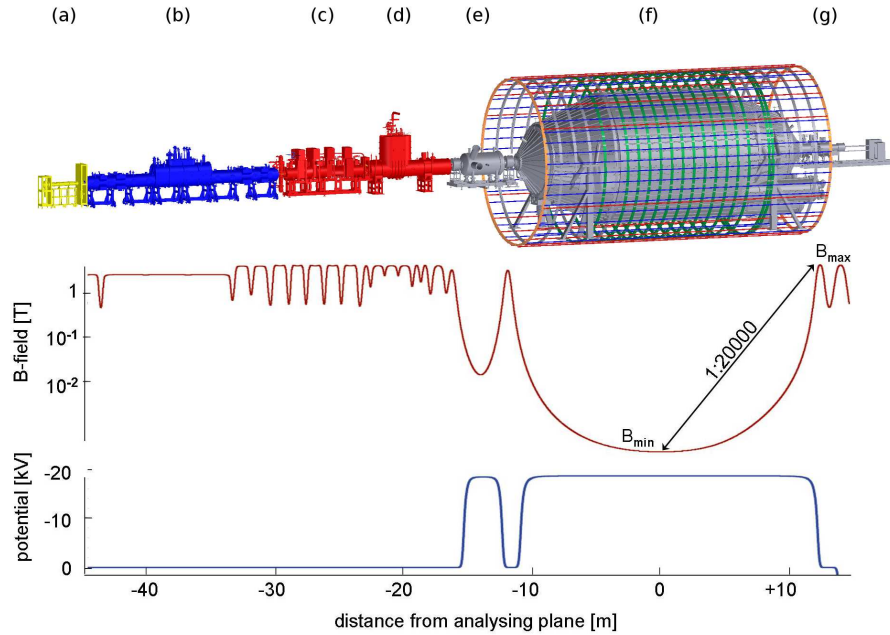


Figure 1. The KATRIN experimental setup with its main components: a, rear section; b, windowless gaseous tritium source (WGTS); c, differential pumping section (DPS); d, cryogenic pumping section (CPS); e, pre-spectrometer; f, main spectrometer with large-volume air coil system; g, focal plane detector. Below, the magnetic field and the electric potential along the beam axis are displayed.

High-purity molecular tritium gas with a temperature of 30 K is injected into the middle of the 10 m long and 9 cm diameter tube of the WGTS (Windowless Gaseous Tritium Source). The injected gas diffuses to both ends of the WGTS beam tube, where it is pumped out to a large degree by a total of 4 pumping ports [9]. A system of 21 superconducting coils generates a high (3.6 T – 5.6 T) magnetic field, which guides the β -decay electrons out of the source along magnetic field lines.

DPS and CPS

The transport section downstream of the WGTS consists of two main tritium retention systems: the DPS (Differential Pumping Section) and the CPS (Cryogenic Pumping Section). Both components together eliminate the remaining tritium gas from the beamline, thus preventing tritium migration to the main spectrometer. This is of major importance, as even trace amounts of tritium in the main spectrometer would cause an intolerably large background rate and initiate large systematic effects, through the β -decays of the tritium molecules. To prevent this, the tritium gas at first is differentially pumped out at the 4 main pump ports of the DPS [10]. Second, the remaining tritium is trapped on to the cold inner surfaces of the CPS [11]. The beam tube of both cryostats is operated at high magnetic fields up to 5.5 T, in order to guide the β -decay electrons towards the main spectrometer. This magnetic field is created by 5 and 7 superconducting coils in the DPS and CPS, respectively. Some of these coils are

not coaxial with the main beamline, in order to reduce the molecular beaming effect [12]. As the transport section also filters out positive ions, only electrons are transmitted to the electrostatic spectrometers for energy analysis.

Pre-spectrometer

At first, a smaller spectrometer (pre-spectrometer) at the entry of the spectrometer section allows to filter out the low-energy part of the β -spectrum which is not important for the neutrino mass determination (since the energy is not close to the endpoint). In fact, the potential of the pre-spectrometer can be adjusted from 0 up to -18.3 kV, thus optimizing the background level as a function of the filter potential [13]. The pre-spectrometer has two superconducting coils at the ends: both of them have a reference field of 4.5 T at the coil centre, and they generate a 15 mT field in the middle of this spectrometer. In the following we refer to the source-side magnet (between CPS and pre-spectrometer) as PS 1 coil, and the other one (between pre- and main spectrometer) as PS 2 coil. Due to the magnetic field of these coils, the β electrons are adiabatically guided through the pre-spectrometer, even when operated at low or zero potential [13].

Main spectrometer

The very large main spectrometer (length 23.6 m, diameter 10 m) has the task of precision energy filtering so that only electrons with high enough kinetic energy are able to overcome the electrostatic retarding potential to be transmitted to the detector for counting. All electrons with smaller kinetic energy are reflected and move back to the source. However, the electric field inside the main spectrometer is able to filter only the longitudinal kinetic energy E_{\parallel} of the electrons, but not the transversal energy E_{\perp} (the longitudinal energy is defined by the electron velocity component parallel to the magnetic field direction). As β -decay electrons in the source are created with isotropic angular distribution, a significant part of their energy can be transversal. If their transversal energy component E_{\perp} remained unaltered, most of the electrons with total energy near the endpoint would not reach the detector, resulting in a rather poor statistics. The solution for this problem is to significantly reduce the magnetic field strength towards the center of main spectrometer. The corresponding field configuration has been designed to first order so that the motion of β -electrons in the KATRIN system is adiabatic [14, 13]. Therefore the first adiabatic invariant (proportional to transversal energy per magnetic field) is approximately constant (see Eq. 1 in the next section for the relativistic expression of this adiabatic invariant). Consequently, when the β -decay electrons move from high to small magnetic field (i.e. from the entry to the centre of the main spectrometer), most of their transversal kinetic energy is converted into longitudinal energy. In doing so, it is important to keep the appropriate order: first the conversion of transversal to longitudinal energy has to take place before the reflecting electric field ‘eats up’ all the longitudinal energy of the electron (see the next section for more details).

Due to the non-zero magnetic field inside the main spectrometer, this conversion is

not perfect, thus the electrons will retain a small transversal energy. As this energy is not scanned by the electrostatic retarding potential, it also defines the energy resolution of the experiment. With a reference value of the magnetic field in the middle of the main spectrometer of 0.3 mT (which is 20000 times smaller than the maximal field of 6T in the KATRIN setup), the energy resolution of KATRIN (defining the width of transmission from 0 \rightarrow 100 % for an isotropic source) will be 0.93 eV at 18.6 keV electron energy.

The conversion from transversal to longitudinal energy is also called magnetic adiabatic collimation (the electron velocity directions are collimated parallel to the magnetic field), and a spectrometer using electrostatic retardation together with magnetic adiabatic collimation, like the KATRIN main spectrometer, is called a MAC-E filter [15, 16]. Thus the KATRIN experiment, like the pioneering Mainz [17] and Troitsk [18] neutrino mass experiments, will make use of the MAC-E filter principle to measure the neutrino mass.

A β -decay electron coming from the source follows a specific magnetic field line, to a good approximation. Therefore the β -decay electrons created inside the transported magnetic flux tube (defined by the reference magnetic flux value of 191 Tcm²) will always remain inside this flux tube until they are counted by the detector. Since the magnetic field in the main spectrometer will be a factor of 10^4 times smaller than the field B_s in the source, the diameter of the flux tube has to be enlarged by a factor of 100 relative to the source. Therefore, the main spectrometer diameter has to be very large (about 10 m). In order to minimize electron interactions with residual gas molecules, the main spectrometer should also feature an excellent ultrahigh vacuum.

The main spectrometer has 3 nearby superconducting coils: at the source side the abovementioned PS 2 coil, and at the detector side the pinch (PCH) and the detector (DET) coils. The latter two together have a significantly larger magnetic moment than the PS 2 coil alone, therefore the magnetic field of the superconducting coils inside the main spectrometer is asymmetric: it is larger at the detector side than near the source side (note that the stray field of a coil is proportional to its magnetic moment).

Table 1 shows the central axial positions and the typical maximal fields of the 3 superconducting coil systems (WGTS, DPS, CPS) and the 4 superconducting coils (PS1, PS2, PCH, DET). In addition, this table presents the contributions of the various superconducting coil systems to the magnetic field at the center ($z = 0$) of the main spectrometer. In Sec. 5 we explain the negative sign of these field values.

Besides the fields of the s.c. coils, there is a non-negligible contribution from the earth magnetic field whose vertical and horizontal components at the location of the KATRIN experiment are 43.6 μ T and 20.6 μ T, respectively [19, 20, 21]. The 20 μ T earth field value in table 1 represents that component of the horizontal earth magnetic field which is parallel to the spectrometer axis; the horizontal perpendicular earth field component is 5 μ T. These values result from the fact that the KATRIN beamline is aligned almost to south-north direction, with an angle of 14° relative to the horizontal earth field.

Field source	z_c (m)	B_c (T)	B_{z0} (μ T)
Earth	-	-	20
WGTS coil system	-38.87	3.6	-9.7
DPS coil system	-27.25	5	-16.3
CPS coil system	-20.58	5.6	-38.2
PS 1 coil	-16.46	4.5	-18.5
PS 2 coil	-12.10	4.5	-46.5
PCH (pinch) coil	12.18	6	-65.2
DET (detector) coil	13.78	3.6	-48.4

Table 1. Axial magnetic field contributions B_{z0} at the center of main spectrometer ($z = r = 0$) from the horizontal earth field and from the various superconducting coil systems and coils. z_c is the central axial position of the coil system, and B_c is the typical maximal field near this position.

In addition to the coils and the earth field, the magnetic field in the main spectrometer can be distorted by magnetic materials in the spectrometer building surrounding the spectrometer vessel. In particular, parts of the concrete reinforcements in the building contain normal steel. In this context it should be emphasized that extensive careful design works were performed, prior to construction of the building, to reduce these effects by employing stainless steel reinforcements (mainly below the spectrometer vessel), to minimize the influence of magnetic field disturbances due to normal steel [22]. Extensive field measurements inside the spectrometer tank [19, 23] have revealed the success of these measures, as the magnetic field in the middle plane of the tank due to the remanent magnetization of the magnetic materials is smaller than 2μ T.

The whole inner surface (700 m^2) of the main spectrometer tank is covered by a wire electrode system to reduce the background due to secondary electrons coming from cosmic muon interactions in the vessel hull, and also to refine and stabilize the electric field inside the tank. This wire system consists of 240 wire modules, with a total wire length of 42 km [24]. Most of the wire modules have a double wire layer, and only the smaller wire module rings at the entrance and exit regions of the main spectrometer tank (at the steep cone) have a single layer. In the standard electric potential mode the outer and inner wire layers will be on a potential which is 100 V and 200 V more negative than the tank, respectively. Accordingly, the single layer modules will be 100-250 V more positive than the inner wires, in order to fulfill the transmission condition (see sections 3 and 5 for more details).

Detector

The transmitted electrons are counted by a segmented silicon PIN-diode detector with 148 pixels, which is located inside the warm bore of the detector magnet DET [25, 26]. The energy resolution of the detector is better than 1.5 keV (FWHM), which

is sufficient to discriminate signal electrons from continuum background. It is possible to elevate the detector on positive potential (up to 10 kV at present), in order to shift signal electrons into a favorable region-of-interest. The standard central field of the detector coil without using this post-acceleration option is 3.6 T (the value we have used for the simulations in this paper). If the post-acceleration is turned on, one can increase the detector coil field up to 6 T.

3. Adiabatic transmission

The motion of electrons with small transversal energy in the KATRIN main spectrometer is approximately adiabatic (see Ref. [13], sec. 8). Thus they follow the magnetic field lines to very good approximation (apart from a small magnetron drift perpendicularly to the field lines). In addition, the first adiabatic invariant

$$\gamma\mu = \frac{\gamma + 1}{2} \frac{E_{\perp}}{B} \quad (1)$$

is constant during the motion. Here B denotes the magnetic field, E_{\perp} the transversal kinetic energy, $\gamma = 1/\sqrt{1 - v^2/c^2} = 1 + E/(mc^2)$ the relativistic Lorentz factor (with electron mass m and kinetic energy E), while μ denotes the orbital magnetic moment of the electron (see sec. 12.5 of [14]). For the following discussion of electron transmission condition through the main spectrometer, let us consider an electron starting at point \mathbf{P}_s in the source with kinetic energy E_s and polar angle θ_s between velocity direction and magnetic field. The electric potential and magnetic field at this point will be denoted by U_s and B_s , respectively. The kinetic energy E of the electron at an arbitrary point \mathbf{P} along its trajectory can then be calculated from energy conservation: $E_s - eU_s = E - eU$, where U is the electric potential at point \mathbf{P} , and e denotes the unsigned electron charge ($e > 0$). The adiabatic longitudinal energy at point \mathbf{P} is then:

$$E_{\parallel} = E_s + e(U - U_s) - \frac{B}{B_s} \frac{\gamma_s + 1}{\gamma + 1} E_s \sin^2 \theta_s, \quad (2)$$

with magnetic field B at point \mathbf{P} and the relativistic factors γ and γ_s at points \mathbf{P} and \mathbf{P}_s , respectively.

Let us first consider only small starting angles so that $(B/B_s) \sin^2 \theta_s < 1$ is fulfilled everywhere between source and detector (absence of magnetic mirror reflection). In this case, for large enough starting energy E_s , the adiabatic longitudinal energy is positive everywhere along the electron trajectory. This means that the electron is transmitted, i.e. it reaches the detector (assuming adiabaticity). Now, we define the analyzing point \mathbf{P}_A as the point along the magnetic field line where the longitudinal energy has its minimal value. Decreasing the starting kinetic energy E_s , there exists a transmission energy $E_s = E_{\text{tr}}$ so that the longitudinal energy is zero at the analyzing point \mathbf{P}_A , while at other points still being positive. This transmission energy has the expression

$$E_{\text{tr}} = \frac{e(U_s - U_A)}{1 - (B_A/B_s) [(\gamma_s + 1)/(\gamma_A + 1)] \sin^2 \theta_s}, \quad (3)$$

where U_A and B_A denote the electric potential and magnetic field at the analyzing point. It is obvious from the above definition that E_{tr} corresponds to a transmission limit: for starting energies above the transmission energy ($E_s > E_{\text{tr}}$) the electron is transmitted and reaches the detector, while for energies below this limit ($E_s < E_{\text{tr}}$) the electron is reflected back towards the starting point and does not get to the detector. With this definition it is evident that the reflection can occur only before or at the point \mathbf{P}_A , so once the electron propagates to \mathbf{P}_A it will reach the detector. In order to compute the adiabatic transmission energy, the electric potential and magnetic field values at the starting point (U_s and B_s) and at the analyzing point (U_A and B_A) have to be known. Note that, generally, the analyzing point \mathbf{P}_A and therefore also the corresponding U_A and B_A values depend on the starting polar angle θ_s .

The knowledge of the above transmission energy is crucial in order to compute the transmission function, which is the probability that an electron with fixed starting energy is transmitted. The transmission function depends explicitly on the starting energy; in the adiabatic approximation it is an increasing function of E_s (in some regions of E_s it is constant). Importantly, it depends strongly on the starting angle distribution of the electrons (through the θ_s dependence of E_{tr} ; see Eq. 3). To calculate the transmission function, first one has to find (for a given starting energy E_s) the angular transmission region, i.e. those values of θ_s for which $E_{\text{tr}} < E_s$ is fulfilled. Second, one has to integrate the normalized electron angular distribution over this region. Due to the θ_s dependence of U_A and B_A (in the general case) this calculation can be rather complicated.

For zero starting angle ($\theta_s = 0$), the analyzing point is where the absolute potential $|U|$ attains its maximal value (let us denote this point by \mathbf{P}_A^0). In the following we assume that the main spectrometer electrode system displays a mirror symmetry relative to the center ($z = 0$) of the spectrometer vessel. In this case, for the on-axis field line ($r = 0$) the point \mathbf{P}_A^0 is at $z = 0$. For off-axis field lines the axial coordinate of the point \mathbf{P}_A^0 can be different from zero. However, it is zero if the field line is symmetric to the $z = 0$ plane (in that case the radial component of the magnetic field at $z = 0$ vanishes).

On the other hand, for finite starting angles the magnetic field can shift the point \mathbf{P}_A away from \mathbf{P}_A^0 : in this case, the analyzing point \mathbf{P}_A depends on the starting angle θ_s . This can happen if the electric potential is rather homogeneous close to the point \mathbf{P}_A^0 , and the magnetic field has a minimum value at \mathbf{P}_A^0 and is rather inhomogeneous near this point. Namely, in this case the third magnetic field term in eq. 2 decreases the longitudinal energy when the point moves away from \mathbf{P}_A^0 (due to the increasing magnetic field), while the slow increase of the eU term is not able to compensate this decrease. Therefore, the longitudinal energy minimum will not be at \mathbf{P}_A^0 , but somewhere farther away, where the electric potential becomes more inhomogeneous. In this case, the analyzing point \mathbf{P}_A and thus the U_A and B_A values depend on θ_s , and a rather complicated procedure is required to determine the transmission function. In this case we say that the transmission condition — i.e. the independence of the analyzing point from the starting angle — is not fulfilled. Fig. 2 shows an example of the behaviour of

the longitudinal energy E_{\parallel} in case of violation of the transmission condition.

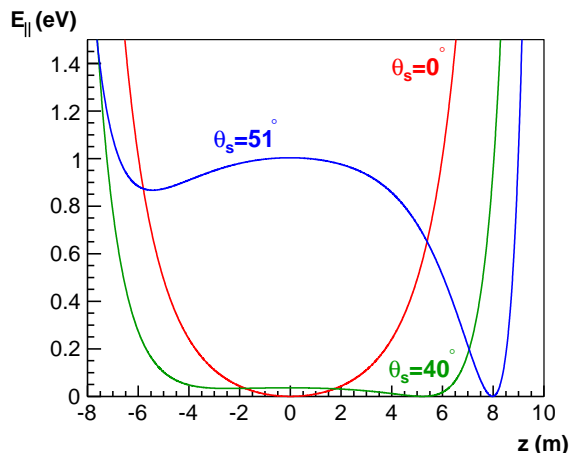


Figure 2. Example for violation of the adiabatic transmission condition for an on-axis field line. The curves display the longitudinal energy for 3 different starting angle values.

The evaluation of the transmission energy and transmission function is much simpler if the analyzing point remains at \mathbf{P}_A^0 for all starting angles. In that case, if we assume that the field lines are symmetric to the $z = 0$ mirror plane, all analyzing points are at the $z = 0$ mirror plane (this is then also called analyzing plane). In addition, the transmission function is determined by the electric potential and magnetic field in the source and the analyzing plane only. To satisfy the $\mathbf{P}_A = \mathbf{P}_A^0$ transmission condition (independence of \mathbf{P}_A from the starting angle), we have two possibilities in the layout of the electromagnetic fields. First, we can improve the homogeneity of the magnetic field near the mirror plane, so that the change of the third magnetic term in eq. 2 becomes smaller than the change of the second electric term. One could also make the electric potential near the mirror plane more inhomogeneous, but then the potential will also be more inhomogeneous in radial direction of the analyzing plane, and this would be disadvantageous for the precise determination of the transmission function. Second, we can use a coil configuration where the magnetic field in the mirror plane does not have a global minimum, but a local maximum instead [27] and two local minima somewhere near the mirror plane. In that case, when moving away from the point \mathbf{P}_A^0 , the third magnetic term in eq. 2 first increases due to the decreasing magnetic field, so that the longitudinal energy also increases. Farther away from \mathbf{P}_A^0 the magnetic field term decreases, but there the second inhomogeneous electric potential term is able to overcompensate the magnetic term. Accordingly, the analyzing point remains in the mirror plane for all starting angles and magnetic field lines. We say that in these two cases the transmission condition is fulfilled.

4. Physical requirements on the magnetic field in the main spectrometer

To optimize the background and transmission properties for the KATRIN experiment, the magnetic field in the main spectrometer has to fulfill certain requirements.

- **Magnetic guidance**

A key task of the magnetic field is to guide the electrons from the source to the detector without electron trajectories touching beam line elements, as this would result in a loss of neutrino mass measurement statistics and in increased background. For this reason, it is required that the flux tube (the bundle of magnetic field lines originating from the source) should fit well inside the main spectrometer tank. Fig. 3 shows the magnetic field lines corresponding to the boundaries of the reference 191 Tcm² flux tube, without the LFCS air coils at the main spectrometer, with only the stray fields of the s.c. solenoids (see Table 1). The left figure a, includes the influence of the earth magnetic field, while the right figure b, assumes that the earth field is fully compensated. In case a, the flux tube is strongly deformed by the earth field, so that a large part of the β -decay electrons from the source would hit the inner walls of the spectrometer and thus would not be detected. In addition, secondary electrons from cosmic muon interactions would be guided to the detector, thus increasing the background over a large part of the flux tube. In case b, the earth magnetic field is assumed to be fully compensated, but the flux tube is still larger than the spectrometer, causing similar problems. Clearly, an additional field shaping element is required to constrain the maximal diameter of the flux tube so that it fits into the vessel geometry.

- **Transmission condition**

The magnetic field configuration generated by the superconducting coils is asymmetric (has no mirror symmetry), so that the transmission condition discussed in Sec. 3 is not fulfilled. This calls for a field-shaping element which allows to compensate the violation of the transmission condition.

- **Homogeneity**

Once the transmission condition is satisfied, the magnetic field values within the analyzing plane should be as homogeneous as possible, so that the transmission function can be determined very precisely.

- **Background**

The magnetic field inside the main spectrometer is of key importance to minimize the cosmic ray μ -induced background. Previous investigations performed with the Mainz neutrino mass spectrometer [28, 29] and the KATRIN pre-spectrometer [30, 31] have revealed that the background is smaller when the magnetic field inside the spectrometer is higher. Namely, secondary electrons emitted at the inner surface of the spectrometer and electrodes cannot easily move perpendicularly to magnetic field lines (they move much easier parallel to these field lines). Accordingly, the magnetic field acts as strong shielding against these electrons. For higher

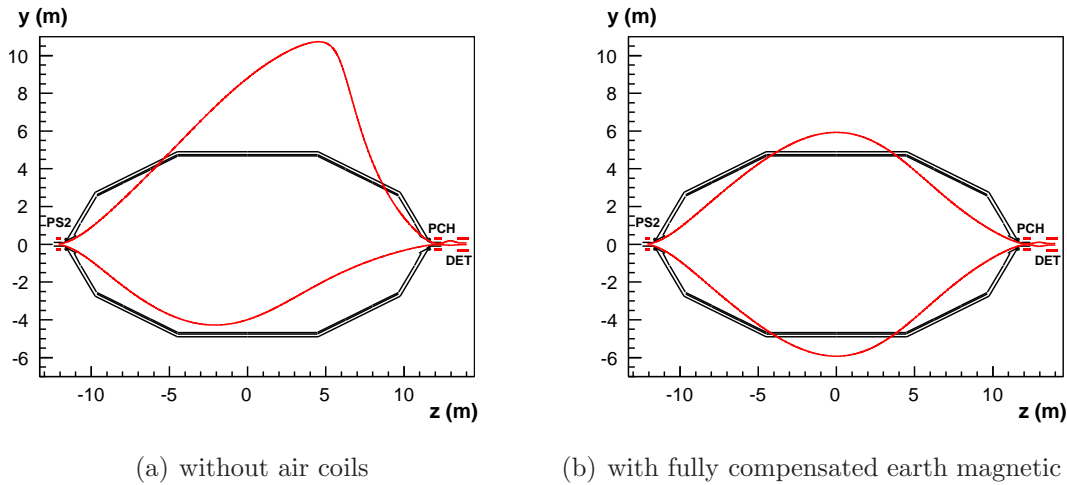


Figure 3. The reference 191 Tcm² flux tube magnetic field lines inside the main spectrometer without LFCS air coils. Displayed is the precise vessel geometry with a steep and flat cone ends and a cylindrical middle part. In case a, the influence of the earth magnetic field has not been compensated, while in case b, it has been assumed to be fully compensated. The y axis corresponds to the vertical direction. For visualization purposes, the radial thicknesses of the coils in these figures are larger than the real values.

values of the magnetic field inside the spectrometer volume the shielding is more efficient, as for example the flux tube then is farther away from the inner tank and electrode surface. It is then also easier to fulfil the transmission condition, as the electric potential is usually more inhomogeneous closer to the spectrometer axis. On the other hand, a higher magnetic field at the analyzing plane reduces the energy resolution, thereby making the transmission function broader. As a result, we get a somewhat smaller signal rate and we have to know more precisely the transmission function. Obviously, one has to find some optimum magnetic field with small background rate and acceptable energy resolution. In addition, a good compensation of the earth magnetic field makes the overall magnetic field in the spectrometer more axially symmetric, and this could also be important to reduce the background. In addition, electron tracking simulations indicate that the background could depend also on the magnetic field shape in the main spectrometer (e.g. one minimum or two minima with local maximum) [32].

Taking into account the above considerations, an additional field-shaping element is required to guarantee an optimized performance of the main spectrometer. This element is the large volume air coil system surrounding the main spectrometer. The system combines two distinct units: the Low Field Correction System (LFCS) to fine-tune the axisymmetric low field part of the magnetic guiding flux tube, and the Earth Magnetic field Compensation System (EMCS). Both systems are described in detail below.

5. The Low Field Correction System (LFCS)

General overview

The LFCS comprises 14 large (12.6 m diameter) air coils arranged coaxially with the main spectrometer tank and the superconducting coils at both ends of the spectrometer (the green circles in Fig. 4). Table 2 lists the axial coordinates z_c , winding numbers N_{turns} and maximal currents I_{max} of the LFCS coils. Due to the large gaps between the neighbouring coils (70 cm or more), there is enough space for accessing various parts of the main spectrometer tank from outside the air coil system. Each coil is driven by its own power supply, so that the currents in each coil can be adjusted individually. As a result, different magnetic field profiles inside the main spectrometer can be implemented on short time scales. This allows for precision fine-tuning of the shape of the magnetic field and for adjusting the total magnetic field strength to various needs.

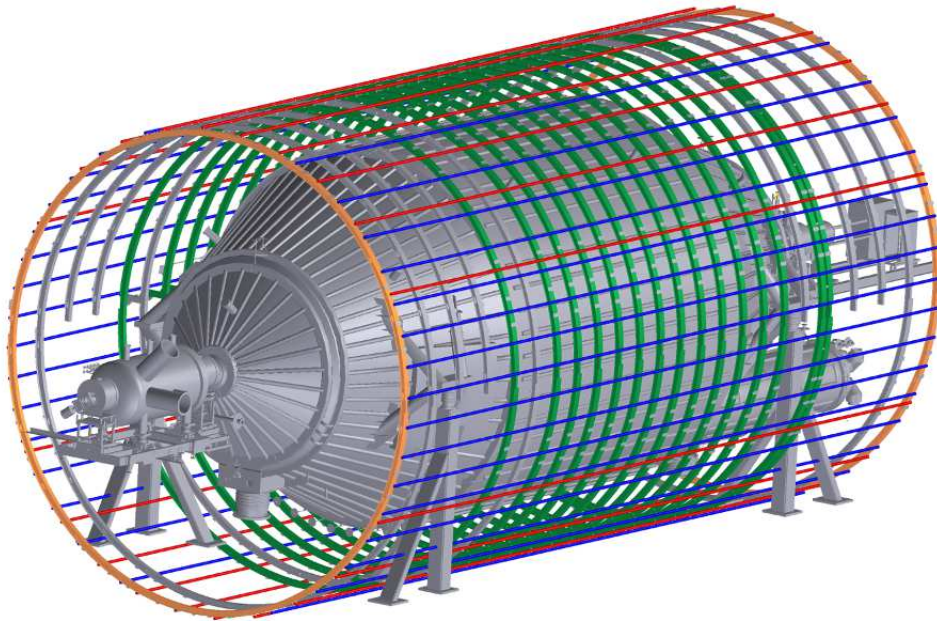


Figure 4. The KATRIN main spectrometer with the large volume air coil system. The green circles represent the LFCS coils. The blue and the red straight lines belong to the current loops of the vertical and the horizontal components of the EMCS, respectively. The two orange circles at the ends contain the current arcs that connect together the linear current sections of the EMCS.

With the help of the LFCS coils we can set the magnetic field value in the middle of the spectrometer to any value up to 1 mT. In normal neutrino mass measurement conditions the magnetic field at the center ($z = 0, r = 0$) of the spectrometer should be larger than a minimum value of 0.33 mT, so that the reference 191 Tcm² flux tube fits into the spectrometer tank. The field of the superconducting coils at the center contributes with about 0.2 mT, therefore the overall magnetic field direction of the LFCS

Coil index	z_c (m)	N_{turns}	I_{max} (A)	I (A) [1 min.]	I (A) [2 min.]
1	-6.79	14	100	-11.2	-0.5
2	-4.94	14	100	-15.3	0.
3	-4.04	8	125	-7.9	-4.8
4	-3.14	8	125	-13.4	-7.1
5	-2.24	8	125	-12.2	-6.6
6	-1.34	8	125	-24.2	-19.4
7	-0.44	8	125	-17.1	-57.2
8	0.46	8	125	-20.3	-51.2
9	1.35	8	125	-18.5	-22.7
10	2.26	8	125	-23.1	-12.5
11	3.16	8	125	-21.9	-7.7
12	4.06	14	100	-18.1	-16.8
13	4.95	14	100	-13.3	-15.9
14	6.6 and 6.9	14 + 14	70	27.3	42.1

Table 2. Optimized LFCS coil currents for 2 different field configurations: 1 global minimum (column 4), and 2 local minima with a local maximum for off-axis field lines (column 5). z_c is the axial position of the coil center, N_{turns} denotes the number of turns, and I_{max} is the maximum current of the constructed coil. Coil 14 is implemented as a double coil, therefore it has 2 different axial positions; both subcoils have 14 turns. All LFCS coils have 6.3 m inner radius, 2 cm radial thickness and 19 cm axial length.

has to be the identical to the field direction of the superconducting coils. If a higher magnetic field in the middle of the main spectrometer is required, the background level is expected to be reduced significantly, but then the transmission function is broader, i.e. the energy resolution is worse.

As outlined above, the field of the superconducting coils is rather asymmetric with regard to the middle plane, since their stray field at the detector side of the main spectrometer is larger than at the source side (see also Fig. 3(b)). With the LFCS it is possible to compensate this asymmetry to a large extent. For this purpose, the LFCS coil 14 at the detector side (see Fig. 6) will be used as a counter coil with a current direction opposite to all other coils. As this task requires a rather large amperturn value, coil 14 consists of 2 parts, each of them having 14 windings with slightly different axial coordinates (see Table 2).

The currents of the LFCS coils have to be optimized so that the transmission condition is fulfilled. This task can best be realized if the superconducting stray field is smaller and the LFCS field is larger. Accordingly, we define the KATRIN magnetic field direction opposite to the horizontal earth magnetic field direction. In this layout, the earth field reduces the stray field of the superconducting coils, as desired. As outlined earlier, a big advantage in this regard is that the main spectrometer axis has approximately a south-to-north direction (detector side is at north). Accordingly, the

axial (z) component of the earth magnetic field has source-to-detector direction ($20 \mu\text{T}$; see table 1). This allows to choose a detector-to-source (negative) direction for the KATRIN magnetic field, in order to reduce the superconducting stray field by the horizontal earth field.

Field optimization

As we have mentioned in the beginning of this section, the LFCS coils allow to adjust many different magnetic field configurations: with various field magnitude values up to 1 mT, with one minimum or two minima field solutions, and with different superconducting fields. In our paper, we present two generic field configurations: first, a configuration with one global magnetic field minimum for all field lines, and second, a configuration with 2 local minima and a local maximum for off-axis field lines. In both cases, the field at the center of the main spectrometer is 0.35 mT. For these calculations we have included the contributions from all superconducting coils of the KATRIN system. Table 1 shows the central axial positions, central fields and field contributions at the main spectrometer center for the 7 superconducting coil systems and coils.

In order to determine the optimized LFCS coil currents, we have used an optimization procedure based on reasonable initial values for the currents. Then we computed the magnetic field lines inside the flux tube (Fig. 6), as well as the magnetic field (Fig. 7) and the adiabatic longitudinal energy (Fig. 8) of an electron along these field lines. Note that these figures correspond to the final optimized current values; in the initial stages of our optimization simulations the parameters looked differently. For example, it occurred that the outer field lines crossed the main spectrometer tank or electrodes, so that one had to increase the absolute value of the LFCS coil currents to increase the magnetic field inside the main spectrometer. If the field lines had a too large diameter in some local region, one had to increase the current values only for the coils near that region. In addition, an important design goal was to set the LFCS currents so that the magnetic field along the field lines (Fig. 7) is approximately symmetric relative to the $z = 0$ plane: in that case one has better chances to fulfill the transmission condition. The latter could be tested by the longitudinal energy figures (Fig. 8). After a few iterations of changing the current values, it was possible to find a configuration which approximately fulfilled the above criteria.

However, after this so called optimization-by-eye procedure, the analyzing points for various starting points and starting angles still had some spread (lying within a region of a few times 10 cm size). In order to reduce substantially the distances between these analyzing points, we used a mathematical optimization method based on several objectives (multiobjective optimization), minimizing the composite objective function by the downhill simplex method [33, 34]. The objective function depends on the 14 LFCS coil currents, therefore the optimization proceeds in this case in a 14 dimensional parameter space. The results of the optimization-by-eye method served as useful starting points for the mathematical optimization procedure. In this way we were able to improve

significantly the transmission properties of the field configurations (see below). We give a detailed explanation of our mathematical optimization method in [Appendix B](#).

Results for two field configurations

Table 2 shows the resulting LFCS coil current values for the two field configurations (1 minimum and 2 minima), based on the abovementioned optimizations. In both cases, the current of coil 14 is positive, i.e. opposite to the sign of all other superconducting and LFCS air coils. In this way the LFCS coil 14 can compensate (at least in the smaller field region) the asymmetry resulting from the larger stray fields of the pinch and detector coils. Fig. 5 shows that the on-axis field without the LFCS coils is larger in the positive z region (detector side); with the LFCS coils this asymmetry becomes smaller. It is also noticeable in table 2 that for the 2 minima configuration the central coils 7 and 8 have to be operated with rather large current values, because in this case the magnetic field is designed to have a local maximum at the center ($z = 0$) of the off-axis field lines.

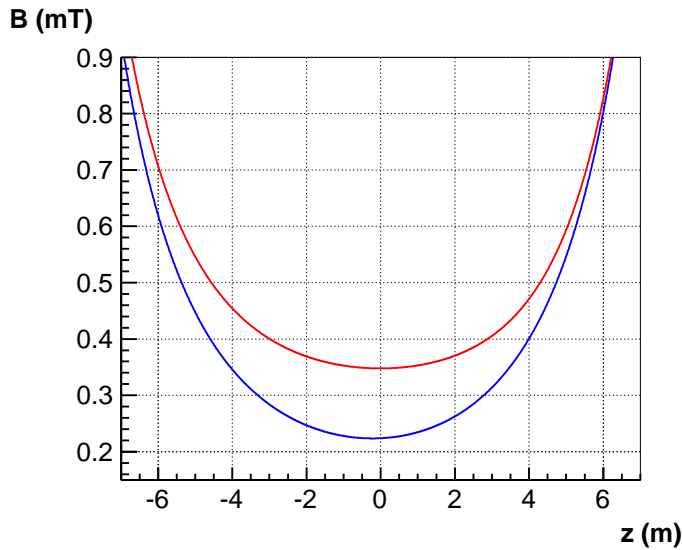


Figure 5. Absolute value of the on-axis magnetic field. The position $z = 0$ corresponds to the center of the main spectrometer. Lower (blue) curve: field of superconducting coils and horizontal earth field alone; upper (red) curve: same as for lower curve, but now the optimized LFCS coils (1 minimum case) have also been included.

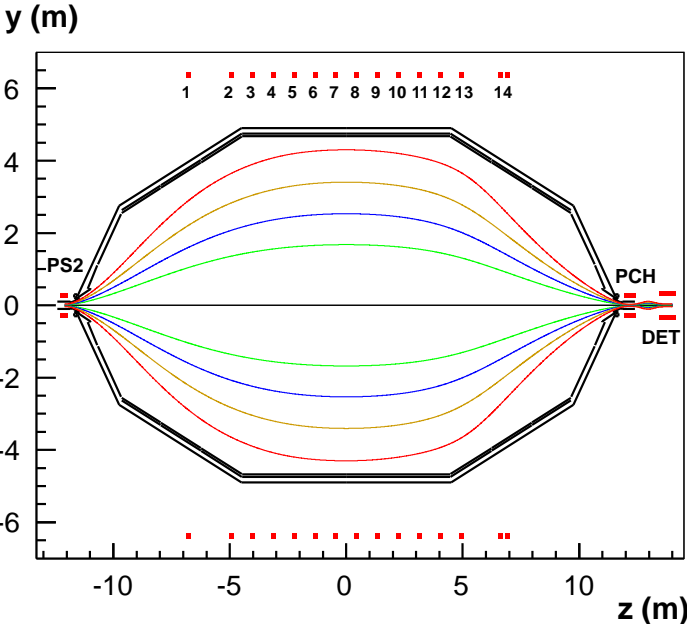
Fig. 6 shows the shape of 5 selected magnetic field lines for both field configurations (1 minimum and 2 minima) after the abovementioned optimizations. In each case the outer field lines correspond to the 191 Tcm^2 flux tube. One can see that the flux tube fits well into the spectrometer tank, in either case with some safety distance (about 40 cm) from the inner wire electrode. Close to the analyzing plane the field lines display a high degree of symmetry relative to the $z = 0$ plane, while farther away at the detector side the field lines attain a smaller diameter than at the source side (due to the higher stray field of the pinch and detector coils). The LFCS coils are also indicated in these

figures by the points at $y = 6.3$ m and $y = -6.3$ m. Only those 3 superconducting coils are displayed here which are closest to the main spectrometer (the PS2, PCH and DET coils at $z = -12$ m, $z = 12$ m and $z = 13.8$ m, respectively).

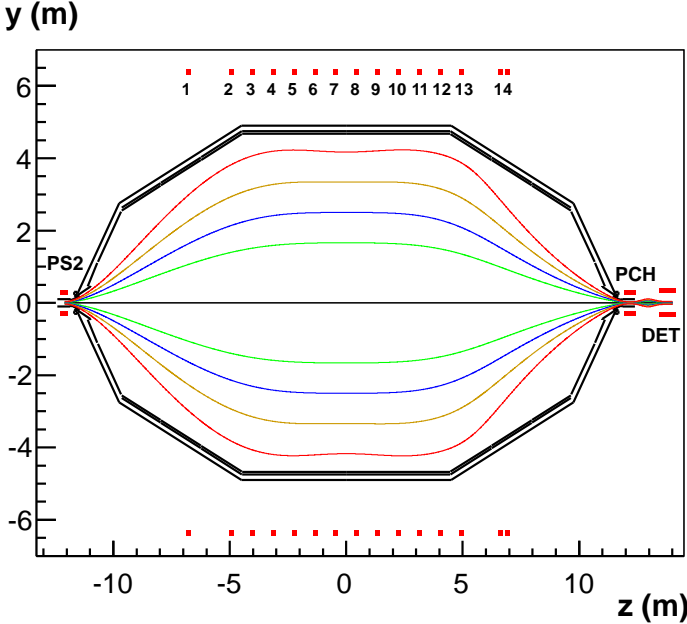
Fig. 7 displays (in an identical color code) the magnetic field strength along the 5 selected magnetic field lines of Fig. 6. Each field line obeys a very good approximate symmetry relative to $z = 0$ (although the field of the superconducting coils alone is quite asymmetric in z -direction), implying that the compensation by the LFCS is successful. In case of the 1-minimum configuration the field has only 1 rather shallow minimum at $z = 0$, while for the “2-minima“ layout this only manifests for the inner field lines (upper curves); the outer field lines (lower curves) experience 2 local minima (a few meters far from the center) and a local maximum at $z = 0$. As explained before, the latter configuration is more reliable from the transmission condition point-of-view. A possible disadvantage of these local field minima is that some electrons with velocities almost perpendicular to the magnetic field could be trapped in these minima. In this way they could cause background by ionizational collisions, in case of sufficient kinetic energy. However, these electrons will be stored anyway by the magnetic mirror trap of the main spectrometer magnetic field, therefore it is unlikely that the local field minima would result in a significant background increase, in comparison to the expected background rate due to the ionizations caused by high energy stored electrons in the main spectrometer [35]. Of course, this specific background issue has to be investigated experimentally.

Fig. 8 shows the longitudinal energy along the same field lines, for electrons starting with the maximal polar angle 51° and with the transmission energy $E_s = E_{tr}$ in the source (WGTS). In both cases, the minimum of the longitudinal energy appears very close to the $z = 0$ symmetry point. To zoom into the critical region-of-interest, we display in Fig. 9 the analyzing points for the minimal and maximal starting polar angles ($\theta_s = 0^\circ$ for the blue lines, $\theta_s = 51^\circ$ for the red lines), but now with a mm scale on the z -axis, for all field lines with $r < 4.2$ m at the center. The analyzing points for intermediate starting angles lie between these two curves. This figure demonstrates that our optimization method for both field configurations results in a very small axial spread of the analyzing points, typically on a scale of a few mm only. It is not meaningful to further improve these analyzing point curves, because small magnetic and electric field disturbances would change these results. For example, the magnetic field of the coils is slightly disturbed by the presence of magnetic materials in the main spectrometer building, and the mirror symmetry of the electric field is affected by the detector-facing pumping ports (which are at the detector side of the main spectrometer), resulting in systematic effects of the same order of a few mm. Taken together, these results imply that the two generic field configurations described above result in a well-defined analyzing plane with a narrow spread in the few mm range, as desired for high-resolution β -spectroscopy.

The final important parameter to be investigated is the radial homogeneity of the magnetic field in the analyzing plane ($z = 0$). In Fig. 10 we can see clear differences



(a) 1 minimum field configuration



(b) 2 minima field configuration

Figure 6. Magnetic field lines inside the main spectrometer (side view), with 0.35 mT field at center. The field lines correspond to the following magnetic flux values (with increasing distance from the axis): 0 Tcm² (black), 30 Tcm² (green), 68 Tcm² (blue), 122 Tcm² (yellow), 191 Tcm² (red). For visualization purposes, the radial thicknesses of the coils in these figures are larger than the real values.

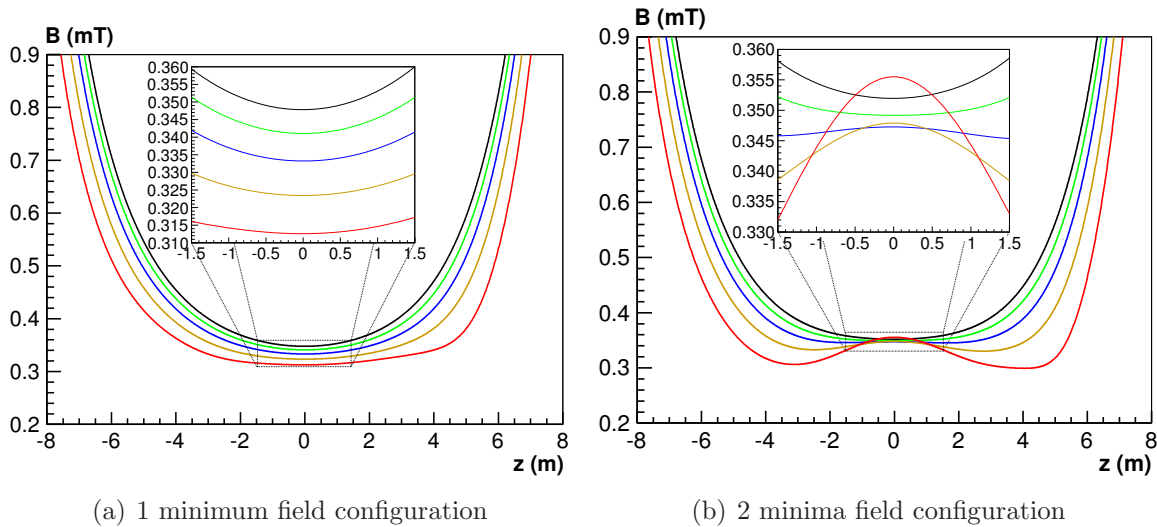


Figure 7. Magnetic field along the field lines of Fig. 6, with 0.35 mT field at center. The colors here correspond to the field line colors of Fig. 6. The insets show the field strength in the innermost part in more detail.

of the two field configurations: the LFCS setup with the 2 minima and local maximum offers a significantly better radial homogeneity than the field configuration with only 1 global minimum. In principle, as outlined above, the magnetic inhomogeneity influences the energy resolution, so a better homogeneity is advantageous. However, this effect can be mapped out to some extent by the segmented focal plane detector [25].

In addition to these two examples of LFCS current setting, we have calculated several other current configurations: scenarios with a higher overall magnetic field in the analyzing plane, and starting configurations with 2 or 4 superconducting coils only. The main spectrometer test experiments, which will be performed in 2013, will use a configuration with only the PS1, PS2, PCH and DET superconducting coils (the WGTS, DPS and CPS are at present still under construction). For these reasons it is important to find optimal LFCS current configurations with stray magnetic fields caused by these 4 superconducting solenoids. One can find optimized LFCS current values for these cases (with many figures) in Refs. [36, 37, 38, 39, 40].

At the end of this section, we mention a possible application of the LFCS for the purpose of background reduction. As outlined in Sec. 2, the MAC-E filter principle of the main spectrometer inherently forms a magnetic mirror trap for high-energy electrons. These trapped electrons undergo many ionizational collisions with residual gas molecules, and the secondary electrons created by these ionizations can cause a significant background increase [35, 39]. A possible method to remove these trapped electrons is by reducing the magnetic field in the middle of the main spectrometer for a short time (e.g. 1 s) down to zero. This is possible by reversing the sign of the LFCS currents. Using this 'magnetic pulse' method [41, 42], all high energy stored electrons are expected to be removed, and this should reduce significantly the background caused by these electrons.

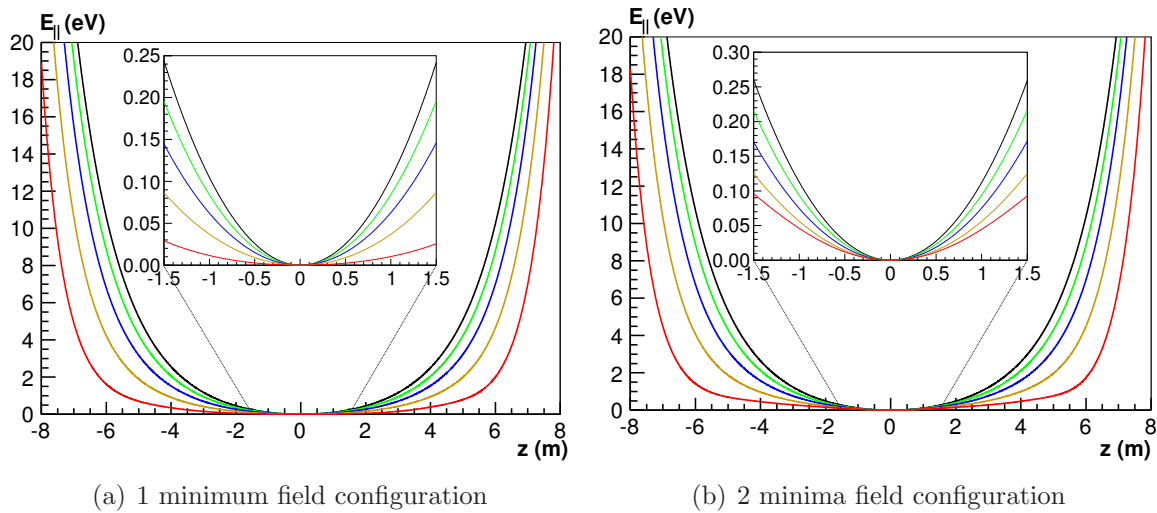


Figure 8. Longitudinal energy distribution along the magnetic field lines of Fig. 6, with 0.35 mT field at center. The colors here correspond to the field line colors of Fig. 6. The electrons were started in the source (WGTS) with transmission energy and with maximal polar angle 51° . For these simulations, most of the wire modules were on vessel potential, except of the two smallest wire module rings at the steep cone part of the main spectrometer, which were 200 V and 300 V more positive than the vessel.

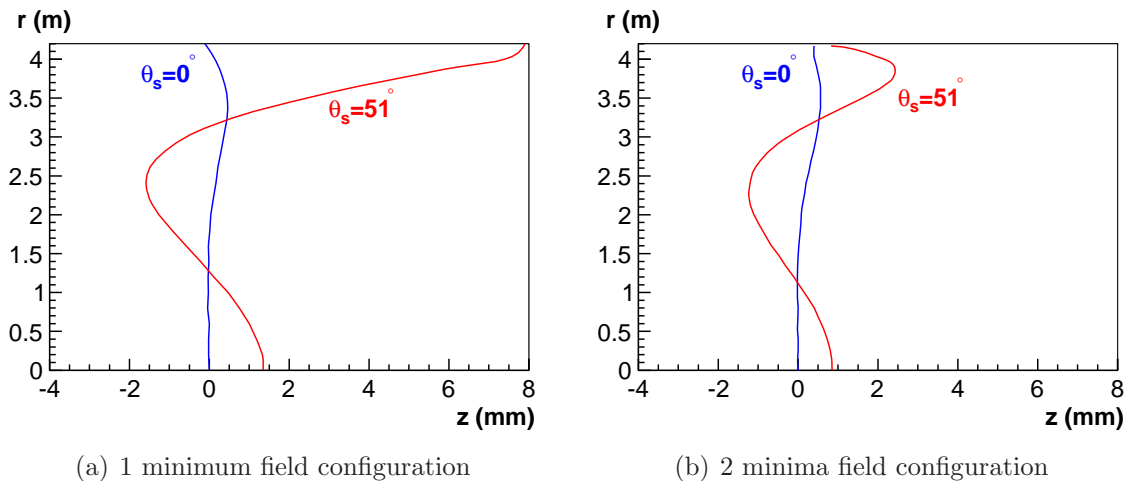


Figure 9. The z and r coordinates of the analyzing points for various field lines and for the minimal and maximal starting polar angles ($\theta_s = 0^\circ$ and $\theta_s = 51^\circ$). Note the scale of the z -axis in mm.

6. The Earth Magnetic field Compensation System (EMCS)

Since the earth magnetic field is homogeneous within the volume of the KATRIN main spectrometer, it is possible to compensate this field distortion with the help of a homogeneous magnetic field. The widely known method to produce such a homogeneous field is by circular or squared Helmholtz-type coil systems [43, 44, 45], where the homogenous field region achieved is, however, significantly smaller than the dimension of the coil system itself. Since the building housing the KATRIN main spectrometer and

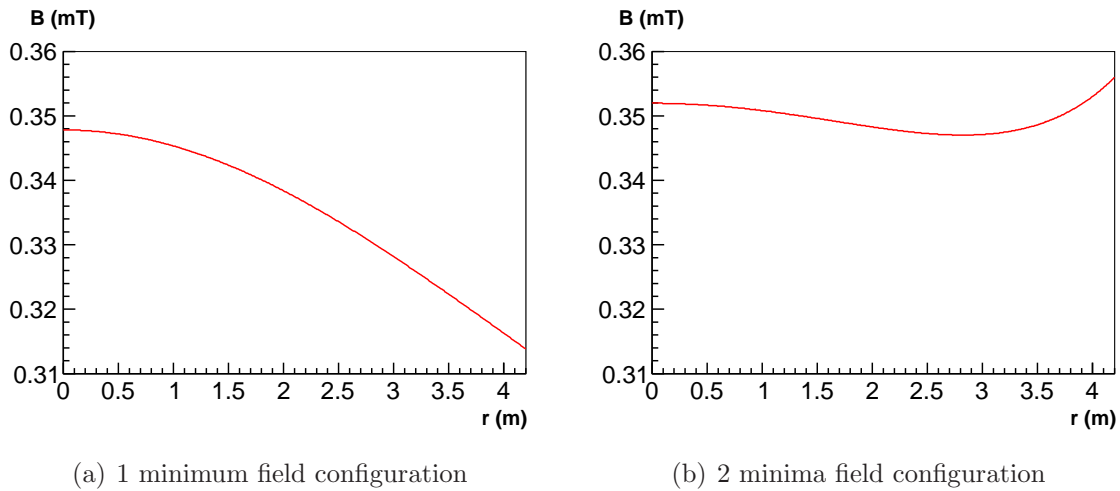
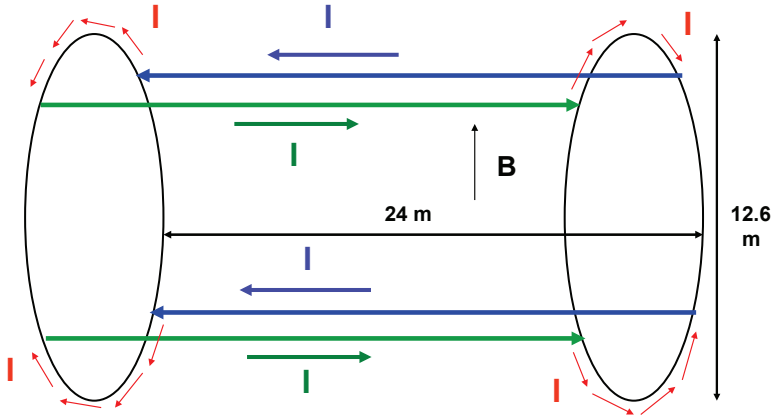


Figure 10. Magnetic field in the analyzing plane ($z = 0$), as function of the radius.

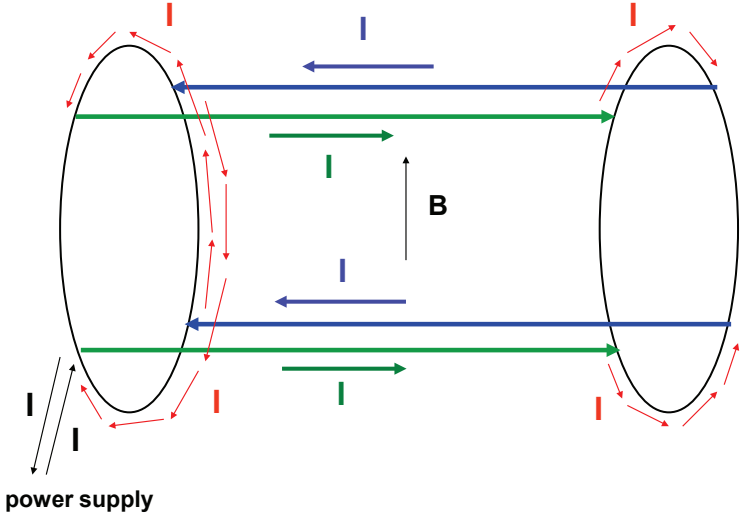
the LFCS system described above offers no extra space, a Helmholtz-type coil method was not a viable method for the earth magnetic field compensation.

Another method to obtain a uniform magnetic field is by spherical cosine coils [46, 47]. The layout of this system relies on the fact that the magnetic field inside a uniformly magnetized sphere is uniform, with the induction vector \mathbf{B} being parallel to the magnetization vector \mathbf{M} [14]. From the point of view of the field intensity \mathbf{H} calculations, the uniform magnetization \mathbf{M} can be replaced by an equivalent surface current distribution $\mathbf{K}_m = \mathbf{M} \times \mathbf{n}$, where \mathbf{n} is the outwardly directed normal vector of the magnetic material surface (see Refs. [48, 49]). Therefore, the equivalent current density is proportional to $\cos \theta_M$, where θ_M is the angle between the normal vector \mathbf{n} and the plane perpendicular to \mathbf{M} . This is the reason for naming this arrangement a cosine coil. In order to build a cosine coil and to get an approximately uniform magnetic field \mathbf{B} inside the coil, the continuous current distribution is replaced by a discrete system of circular current loops, with planes perpendicular to the axis vector \mathbf{B} and positioned equidistantly along the direction of this vector. As one can see in table 3 of Ref. [47], the spherical cosine coil system has a much larger region with a specific level of field uniformity than the simple Helmholtz coil pair.

Unfortunately, a spherical EMCS turned out to be impractical too, due to the above mentioned space restrictions by the spectrometer building. Alternatively, a cosine coil system on the surface of an ellipsoid also features a uniform magnetic field inside the ellipsoid [46, 50]. However, in this case the 3 large vacuum pumps of the main spectrometer tank (see Fig. 1) would have crossed the surface of this ellipsoid, so the ellipsoid solution turned out to be impractical as well. Now, an infinitely long ellipsoid is identical with an infinitely long cylinder, therefore a cosine coil system on the surface of a cylinder can also be used to produce an approximately uniform magnetic field inside the cylinder. In this arrangement, the uniformity of the field increases with the length of the cylinder and with the number of the current loops.



(a) top



(b) bottom

Figure 11. Top: Two horizontal current loops for the compensation of the vertical earth magnetic field component. Bottom: The two current loops united into one coil system.

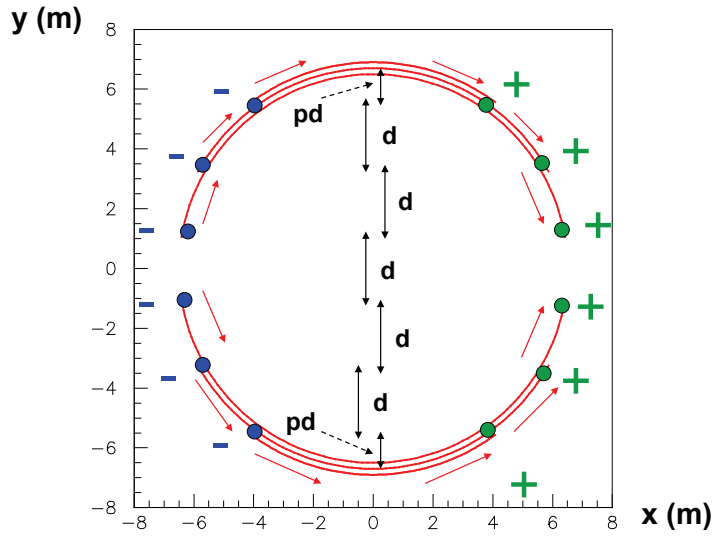


Figure 12. Current flow at an endring of a simplified vertical compensation system with 6 current loops.

Accordingly, an air coil system on the surface of a cylinder surrounding the KATRIN main spectrometer tank turned out to be an optimal solution for the earth magnetic field compensation inside the tank [51, 52, 53]. The length and radius of the cylinder was chosen to be 24 m and 6.3 m, respectively. These dimensions were constrained by the main spectrometer building, and they are identical to the dimensions of the LFCS coils and allow to construct both systems with a single mechanical support structure [6]. In order to compensate the vertical (y) component of the earth magnetic field ($43.6 \mu\text{T}$), we have decided to use 16 current loops with horizontal planes (the blue lines in Fig. 4), and for the horizontal transverse (x) earth field component ($5 \mu\text{T}$) compensation we use 10 current loops with vertical planes (the red lines in Fig. 4). Fig. 11(a) shows a current loop pair that provides a homogeneous vertical magnetic field at the center of the cylinder. One loop contains two linear current sections (both of them parallel with the main spectrometer axis) and, at the two endrings of the cylinder, two arcs that connect the linear sections, rendering the loop a closed current system. Fig. 11(b) shows that the two closed loops are equivalent to one closed current system that is easier to realize practically. Similarly, the 16 current loops of the vertical system and the 10 loops of the horizontal system are integrated into two independent closed current systems. Thus, the EMCS has only two adjustable currents: 50 A to produce a $43.6 \mu\text{T}$ field with the vertical system, and 9.1 A to produce a $5 \mu\text{T}$ field with the horizontal system.

Fig. 12 illustrates the current arcs at one of the endrings in the special case of 6 loops. The positive signs mean that the current in the linear sections, which here are perpendicular to the page, flows in the direction inside the page, and the minus signs

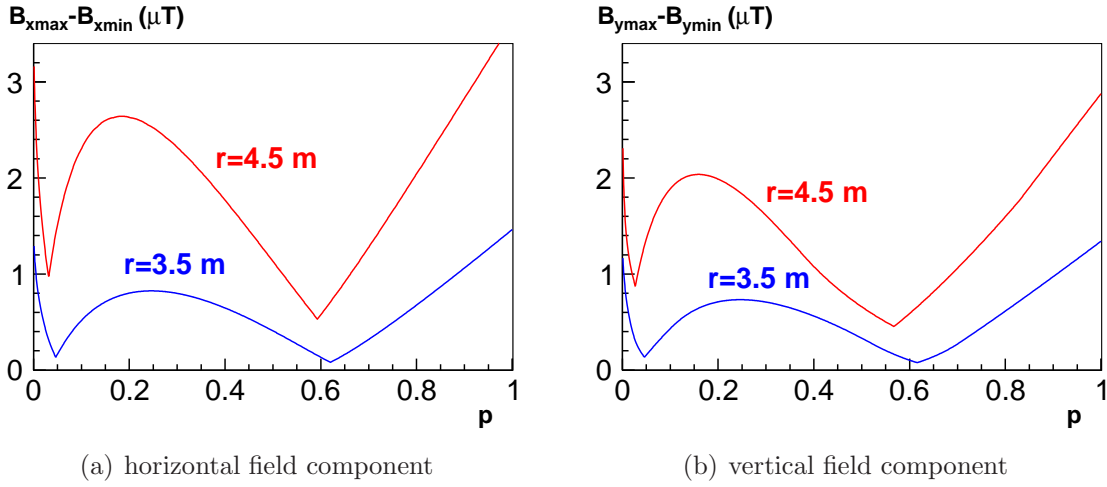


Figure 13. Magnetic field inhomogeneity of the vertical part of the EMCS at the analyzing plane, as a function of the end parameter p , for two different circles (with 3.5 m and 4.5 m radii).

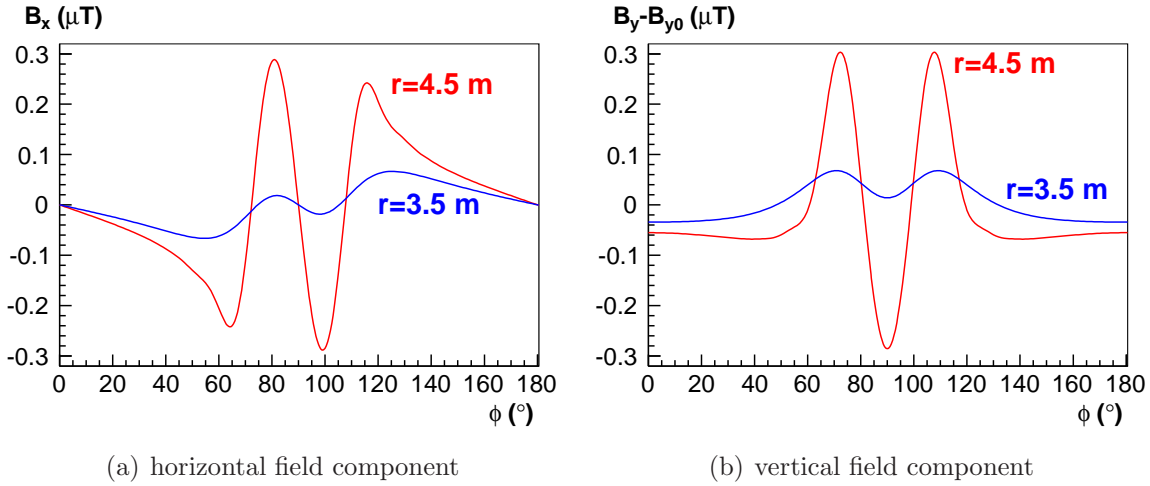


Figure 14. The horizontal magnetic field component B_x and the vertical field component difference $B_y - B_{y0}$ of the vertical compensation system, as function of the azimuthal angle ϕ at two different circles (with 3.5 m and 4.5 m radii) in the analyzing plane. $\phi = 0$ corresponds to the right-hand side point $x = 6.3$ m, $y = 0$ of Fig. 12; $\phi = 90^\circ$ is for the top side point $x = 0$, $y = 6.3$ m. The parameter $B_{y0}=43.6$ μT is the vertical field component of the vertical compensation system at the center of the analyzing plane.

indicate current flow direction outside the page (towards the reader). This figure shows that the current loop planes are equidistant (with distance d). Identical current values of the equidistant loops correspond to an approximation of the cosine current distribution and thus to uniform magnetic field. An important design parameter of the EMCS is given by the so called end parameter p . As can be seen in Fig. 12, the parameter $p \cdot d$ defines the distance of the outermost current loop to the top or bottom of the ring elements, in case of equidistant arrangement of the current loops. Accordingly, p is a

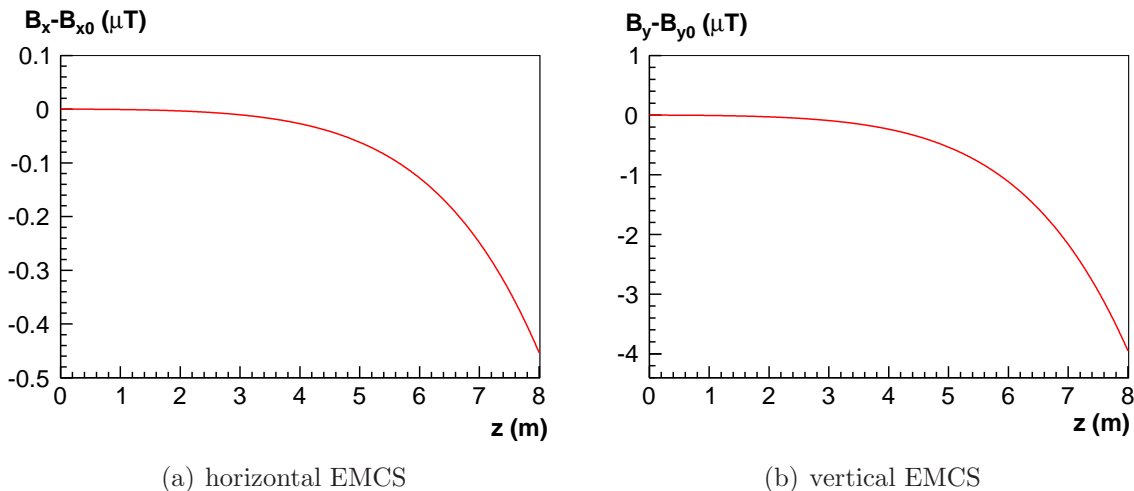


Figure 15. On-axis magnetic field differences of the horizontal (left) and vertical (right) compensation systems, as function of the distance z from the analyzing plane. $B_{x0}=5 \mu\text{T}$ is the horizontal x -component of the horizontal compensation system, $B_{y0}=43.6 \mu\text{T}$ is the vertical y -component of the vertical compensation system, both at the center of the analyzing plane.

dimensionless free parameter with $0 \leq p \leq 1$ [47]. Then, figs. 13(a) and 13(b) show the inhomogeneity of the magnetic field components B_x and B_y of the vertical (y -direction) compensation system at two circles with radii 3.5 m and 4.5 m, as function of the end parameter p (here the inhomogeneity has been defined as the difference of the maximal and minimal field values on the circle). One can see that the best field homogeneity is obtained for $p = 0.6$. Accordingly, we have chosen this value for both the vertical and the horizontal compensation systems. Note that this optimal value of p for a cylindrical cosine coil system is different from the corresponding optimal p values of a spherical cosine coil system [47].

Figure 14 illustrates the field inhomogeneity of the vertical compensation system at the analyzing plane as a function of the azimuthal angle ϕ for two different radii. Note that $\phi = 0$ corresponds in Fig. 12 to the point $x = 6.3 \text{ m}$, $y = 0$. One can see that the inhomogeneity increases with the distance from the spectrometer axis (at a radial position of $r = 4.5 \text{ m}$ from the axis the inhomogeneity is several times larger than at $r = 3.5 \text{ m}$). The inhomogeneity of the field is maximal at the top and bottom region of the coil system (at $\phi = 90^\circ$ and $\phi = 270^\circ$, respectively), where the deviation of the discrete coil setup from the continuous $\cos\theta$ current distribution is maximal. Note that the vertical and the horizontal field components have roughly the same level of inhomogeneity. The actual level of inhomogeneity of less than $0.3 \mu\text{T}$ in the analyzing plane, in comparison with the vertical and horizontal components of the earth magnetic field, and in particular in relation to the absolute value of the guiding field of 0.35 mT , demonstrates the success of our optimization strategy in designing an effective EMCS.

The final important aspect of the EMCS design is the field behaviour along the longitudinal z -axis. In this regard it is important to recall that the distorting effects of

the earth magnetic field have to be compensated mainly in the low field region $|z| < 7$ m. Figure 15 shows that the field inhomogeneity of the horizontal and vertical compensation systems increases with the distance from the analyzing plane (which is also the center of both the vertical and the horizontal coil system). This increase is due to the finite length of the coil systems and due to the field disturbance from the circular current segments of the endrings. The lower quality of the compensation systems near the endrings should not cause any problem, since the magnetic field in the regions $|z| > 7$ m is already much larger than the earth magnetic field (see Fig. 7).

The EMCS is useful not only to compensate the earth magnetic field, but also offers the useful possibility to shift the magnetic flux tube. The vertical and horizontal parts of the EMCS allow shifting the flux tube in the vertical and the horizontal direction by 0.5 m, with 75 A and 50 A current, respectively [53]. These flux tube shifts can be important in order to correct some small transversal shifts of the flux tube in the transport system, and also for specific background investigations and optimizations.

7. Conclusion

The KATRIN experiment will determine the absolute neutrino mass scale down to 200 meV (90 % CL) by measuring the integral electron energy spectrum close to the endpoint of molecular tritium beta decay. The β -electrons are guided from the source to the detector by magnetic fields, typically reaching values in the few T range in the source and transport system and being created by many superconducting coils. The energy filtering of the electrons takes place inside the large volume main spectrometer, which is at high negative potential (around -18.6 kV). In order to convert the transversal energy of the electrons into longitudinal energy by the inverse magnetic mirror effect and thus to improve significantly the efficiency of the energy filtering, the magnetic field strength in the main spectrometer must reach very low values below 0.5 mT. The stray field of the superconducting coils alone is not sufficient to obtain the minimal 0.3 mT field that is needed to constrain the magnetic flux tube to the geometry of the main spectrometer vessel. Moreover, the earth magnetic field disturbs significantly this central low magnetic field region where the energy analysis takes place. The task of the KATRIN large-volume air coil system described in this paper is to fine-tune and compensate these fields.

The LFCS (Low Field Correction System) part of the air coil system consists of 14 coils arranged coaxially with the main spectrometer vessel and the adjacent superconducting coils. With its help it is possible to set the magnetic field inside the main spectrometer from zero up to 1 mT. The homogeneity of the field in the analyzing plane can also be improved considerably. In addition, the asymmetric field of the superconducting coils can be compensated, thus making the field more symmetric relative to the $z = 0$ analyzing plane. Even more importantly, with the LFCS one can fine-tune the magnetic field shape, adjusting it to the electric potential, so that the adiabatic transmission condition is fulfilled. Thus it is much easier to evaluate accurately

the transmission function of the MAC-E filter. The precise knowledge of this function is an essential pre-requisite for a precision scanning of the integral energy spectrum. To fulfill the transmission condition, two different possibilities have been worked out: a magnetic field with a global minimum in the analyzing plane, and a field with a local maximum there but with two local minima a few meters away. The second option has better theoretical properties: an easier fulfillment of the transmission condition and better homogeneity in the analyzing plane. In order to find the optimal LFCS current values corresponding to these field alternatives, we have used a relatively simple and fast mathematical optimization method, based on a composite objective function with multiple objectives.

The second part of the air coil system is the EMCS whose task is to compensate those components of the earth magnetic field which are perpendicular to the spectrometer axis. It consists of two cosine coil systems: one of them compensates the vertical earth magnetic field component ($43.6 \mu T$), the other one compensates the horizontal transversal earth field component ($9.1 \mu T$). In the analyzing plane of the main spectrometer, both the vertical and the horizontal components can be compensated with $0.3 \mu T$ maximal inaccuracy, which is fully sufficient for high-precision β -spectroscopy.

The air coil system was constructed in 2009-2010. Details about its mechanical and electrical layout, and about the commissioning field measurements and comparisons with simulations will be presented elsewhere [6].

The KATRIN large volume air coil system will be an important experimental component for the main spectrometer commissioning measurements, which will start in the first half of 2013. The purpose of these measurements is to examine and reduce the background, and to investigate the electric, magnetic and electron transmission properties of the main spectrometer. With the help of the LFCS and EMCS, one can set magnetic fields inside the main spectrometer in a highly versatile manner by adjusting both the overall field strength as well as the field shape. Presumably, the background and transmission properties of the main spectrometer depend strongly on the LFCS and EMCS currents, and we expect to find current values that result in a rather small background rate and well understood transmission function, in order to obtain optimal conditions for the KATRIN neutrino mass measurements.

Acknowledgements

This research was supported by the Helmholtz Association (HGF), the German Federal Ministry of Education and Research (BMBF), through grants 05A08VK2 and 05A11VK3, and the German Research Foundation (DFG) within the framework of the Transregio project 'Neutrinos and Beyond', grant SFB/TR27. B.L., S.M. and N.W. thank the Karlsruhe House of Young Scientists (KHYS) for supporting part of this study. We would like to thank Tudor Cristea-Platon and Nils Stallkamp for their useful participation in the mathematical optimization computations, and Michaela Meloni for her helping us to create some of the figures.

Appendix A. Field simulations

In this work various field simulation codes have been used for the air coil design. The PartOpt code [54] uses elliptic integrals for magnetic field calculations of axisymmetric coils. In addition, the zonal harmonic expansion method was employed [55, 56]. The latter method can be 100-1000 times faster than the more widely known elliptic integral method and is more general than the similar radial series expansion. It features not only high computational speed but also high accuracy, which makes the method appropriate especially for trajectory calculations of charged particles.

We could not use elliptic integrals or the zonal harmonic expansion to simulate the EMCS since it is not axisymmetric. Instead, the magnetic field of the linear current sections was computed by integrated Biot-Savart formulas [59]. The arcs at the endrings were approximated by many short linear current segments.

In order to compute the adiabatic longitudinal energy, transmission energy and the analyzing points, we also performed electric potential calculations. For this purpose, the boundary element method (BEM) was applied [57, 58]. With BEM, one has to discretize only the two-dimensional surface of the electrodes, and not the whole three-dimensional space of the electrode system, as is the case when using the finite difference and finite element methods [57]. BEM is especially advantageous for electrodes exhibiting small-scale structures within large volumes, like the KATRIN wire electrode system [24]. Inside the flux tube, the electric potential of the main spectrometer wire electrode system is approximately axisymmetric, and with the knowledge of the charge densities from the BEM calculations it is possible to use the zonal harmonic expansion method also for the electric potential computations [60, 56].

The field calculation C codes, written by one of us (F. G.), have been rewritten into C++ code [58, 59] and included into the KASSIOPEIA package that is now the standard simulation framework of the KATRIN experiment [61, 62].

Appendix B. LFCS current calculation by mathematical optimization

Optimization problems naturally arise in many different disciplines, like statistics, engineering, management, empirical sciences etc. In mathematical (numerical) optimization [63, 64, 65], first one has to formulate the problem. This is achieved by defining the design (optimization, decision) variables and the objective (goal or cost) function that has to be optimized (usually with some constraints on the design variables). Then the optimal values of the design variables leading to a minimum of the objective function have to be found by applying some appropriate minimization technique. For more advanced problems, one has typically several different goals and several requirements to be fulfilled simultaneously. In this case one uses multiobjective (vector) optimization, with several objectives to be optimized. One of the possibilities to formulate this kind of optimization problem is by introducing a composite objective

function F as the weighted sum of the objectives O_k :

$$F = \sum_{k=1}^N w_k O_k. \quad (\text{B.1})$$

The weights w_k have to be used so that the best result for the problem is obtained. The most important objectives and those with smaller scalings need larger weight factors, so that these objectives should decrease significantly during the optimization procedure.

In our case, the design variables are the 14 LFCS currents. The magnetic field with the optimal current values has to fulfill several different requirements, therefore we have adopted the multiobjective optimization procedure with composite objective function. For the simulations yielding the results of Sec. 5 we have used $N = 3$ objectives.

Our first objective was the squared deviation of the magnetic field value at the main spectrometer center from an input value: $O_1 = (B_0 - B_{\text{input}})^2$, where $B_0 = B(z = 0, r = 0)$; in our work we have used a value of $B_{\text{input}} = 0.35$ mT.

Our next goal was to find a configuration where the magnetic field and the field lines are approximately perpendicular to the $z=0$ mirror plane. In this case one can expect that the analyzing points are very close to this plane. Therefore, for the second objective we have defined an ensemble of $n = 10$ points at the $z = 0$ mirror plane with $r_p = 0.43 p$ radius values (in meters) ($p = 1, \dots, n$), and we have computed the radial magnetic field components $B_r(p)$ at these points. The second objective O_2 was then defined as the maximum of the $|B_r(p)|$ values.

As for axisymmetric fields the radial component on the axis ($r = 0$) is always zero, we have used also a third objective. The goal here was to have a magnetic field with extremum values in the $z = 0$ plane. For this purpose, we have defined the set of 11 points with $r_p = 0.43 p$, ($p = 0, \dots, n$), and we have computed there the axial gradient field components $\partial_z B(p)$. Then, the third objective O_3 was defined as the maximum of the $|\partial_z B(p)|$ values. For the computation of the axial gradients we used numerical differentiation: $\partial_z B(p) \approx [B(z = \varepsilon, r = r_p) - B(z = -\varepsilon, r = r_p)]/(2\varepsilon)$, with $\varepsilon = 0.1$ mm.

In the next step, the composite objective function is the weighted sum of these 3 objectives (see Eq. B.1 for $N = 3$). We have chosen to use the empirical weight factors $w_1 = 1$, $w_2 = w_3 = 10$.

The points where we have computed the magnetic field values are fixed (they are independent of the optimization procedure), therefore we have been able to reduce significantly the required computation time by calculating, in the beginning, for all points the magnetic field contributions b_j of the LFCS coil j with 1 A current. Then, during the optimization, the field can be computed rapidly as the linear superposition $B = B_{\text{sc}} + \sum_{j=1}^{14} b_j I_j$, where B_{sc} denotes the field due to the superconducting coils and the horizontal earth magnetic field.

To minimize the objective function F , starting at some point in the 14 dimensional current space, we have used the Nelder-Mead downhill simplex method ([33], and [34], sec. 10.4). This popular minimization method requires only the evaluation of functions,

and not their derivatives. It is based on the notion of a simplex that is a geometrical figure having $n + 1$ points (vertices) in the n -dimensional design variable space (the simplex is the generalization of a triangle or tetrahedron for higher dimensions). In the beginning, a simplex is created near the starting point, and it is changed by various transformations (reflection, contraction, expansion, shrinkage) so that the average function value at the simplex vertices continuously decreases, until the simplex attains a local minimum of F where no further significant reduction of the function value is possible.

From the technical point of view, the LFCS currents are not allowed to exceed the upper limits presented in Table 2. In our work, we used the following limits: $I_{\min} = -100$ A, $I_{\max} = 0$ for coils 1-13, $I_{\min} = 0$, $I_{\max} = 70$ A for coil 14. In order to include these limits as constraints into our optimization code, we introduced the following variable transformation: $I_j = I_{\min,j} + (I_{\max,j} - I_{\min,j}) \cdot (1 + \cos x_j) / 2$. Using the variables x_j for the function minimization, instead of the currents I_j , the constrained optimization is turned into the easier case of unconstrained optimization (the variables x_j can have arbitrary values, while the currents are constrained between their lower and upper limits).

As we have mentioned in Sec. 5, the starting point for our mathematical optimization procedure was the result of a first, rough optimization-by-eye operation. We tried our mathematical optimization process also by arbitrary (randomly chosen) starting points. In that case, too, the minimization by the simplex method was able to reduce significantly the objective function value and found some local minimum. Unfortunately, in this case the current values of the neighbouring coils corresponding to these local minima featured rather large jumps, resulting in unnecessarily large currents for some of the coils. Probably, one has to use some additional objectives (like the total electric power of the coils) to avoid these large current jumps. These on-going investigations, however, will not influence our conclusions presented above.

References

- [1] J. Lesgourgues and S. Pastor, Neutrino Mass from Cosmology, *Advances in High Energy Physics*, Vol. 2012 (2012) Article ID 608515. ([hyperlink](#))
- [2] A. Giuliani and A. Poves, Neutrinoless Double-Beta Decay, *Advances in High Energy Physics*, Vol. 2012 (2012) Article ID 857016. ([hyperlink](#))
- [3] E. W. Otten and C. Weinheimer, Neutrino mass limit from tritium β decay, *Rep. Prog. Phys.* 71 (2008) 086201. ([hyperlink](#))
- [4] G. Drexlin et al., Current Direct Neutrino Mass Experiments, *Advances in High Energy Physics*, Vol. 2013 (2013) Article ID 293986. ([hyperlink](#))
- [5] J. Angrik et al. (KATRIN Collaboration), KATRIN Design Report 2004, *Wissenschaftliche Berichte FZKA 7090*. ([hyperlink](#))
- [6] J. Reich et al., Technical design and commissioning of the KATRIN large volume air coil system (in preparation).
- [7] J. Wolf, The KATRIN neutrino mass experiment, *Nucl. Instrum. Meth. A* 623 (2010) 442. ([hyperlink](#))
- [8] T. Thümmler, Direct neutrino mass measurements, *Physics of Particles and Nuclei* 42 (2011) 590. ([hyperlink](#))

- [9] M. Babutzka et al., Monitoring of the operating parameters of the KATRIN Windowless Gaseous Tritium Source, *New J. Phys.* 14 (2012) 103046. ([hyperlink](#))
- [10] S. Lukic et al., Measurement of the gas-flow reduction factor of the KATRIN DPS2-F differential pumping section, *Vacuum* 86 (2012) 1126. ([hyperlink](#))
- [11] W. Gil et al., The cryogenic pumping section of the KATRIN experiment, *IEEE Trans. Appl. Supercond.* 20 (2010) 316. ([hyperlink](#))
- [12] X. Luo et al., Monte Carlo simulation of gas flow through the KATRIN DPS2-F differential pumping system, *Vacuum* 80 (2006) 864. ([hyperlink](#))
- [13] M. Prall et al., The KATRIN pre-spectrometer at reduced filter energy, *New Journal of Physics* 14 (2012) 073054. ([hyperlink](#))
- [14] J. D. Jackson, *Classical Electrodynamics* (John Wiley & Sons, New York, 1999).
- [15] V.M. Lobashev and P.E. Spivak, A method for measuring the electron antineutrino rest mass, *Nucl. Instrum. Meth. A* 240 (1985) 305. ([hyperlink](#))
- [16] A. Picard et al., A solenoid retarding spectrometer with high resolution and transmission for keV electrons, *Nucl. Instrum. Meth. B* 63 (1992) 345. ([hyperlink](#))
- [17] Ch. Kraus et al., Final results from phase II of the Mainz neutrino mass search in tritium β decay, *Eur. Phys. J. C* 40 (2005) 447. ([hyperlink](#))
- [18] V. M. Lobashev, The search for the neutrino mass by direct method in the tritium beta-decay and perspectives of study it in the project KATRIN, *Nucl. Phys. A* 719 (2003) 153c. ([hyperlink](#))
- [19] J. Reich, Magnetfeldmessungen und Designarbeiten für das EMCS Luftspulensystem am KATRIN Hauptspektrometer, Diploma thesis, KIT, 2009. ([hyperlink](#))
- [20] S. Macmillan and S. Maus, International Geomagnetic Reference Field - the tenth generation, *Earth Planets Space* 57 (2005) 1135. ([hyperlink](#))
- [21] On-line calculators to estimate current and past values of the magnetic field, International Geomagnetic Reference Field, NOAA, National Geophysical Data Center. ([hyperlink](#))
- [22] F. Glück, Steel in the KATRIN buildings and the magnetic field in the main spectrometer, KATRIN internal report 2005, KATRIN BSCW 25-51. ([hyperlink](#))
- [23] J. Reich, Magnetic Field Inhomogeneities and their Influence on Transmission and Background at the KATRIN Main Spectrometer. Dissertation, KIT, 2013. ([hyperlink](#))
- [24] K. Valerius, The wire electrode system for the KATRIN main spectrometer, *Progress in Particle and Nuclear Physics* 64 (2010) 291. ([hyperlink](#))
- [25] F. Harms, Assembly and First Results of the KATRIN Focal-Plane Detector System at KIT, Diploma thesis, KIT, 2012. ([hyperlink](#))
- [26] J. F. Amsbaugh et al., Focal-plane detector system for the KATRIN experiment, to be submitted to *Nucl. Instrum. Meth. A*.
- [27] F. Glück et al., The neutron decay retardation spectrometer aSPECT: Electromagnetic design and systematic effects, *Eur. Phys. J. A* 23 (2005) 135. ([hyperlink](#))
- [28] D. Goldmann, Untersuchung systematischer Streffekte auf das β -Spektrum im Mainzer Neutrinoruhemassenexperiment, Diploma thesis, University of Mainz, 1995.
- [29] B. Müller, Umbau des Mainzer Neutrinomassenexperiments und Untergrunduntersuchungen im Hinblick auf KATRIN, Diploma thesis, University of Mainz, 2002. ([hyperlink](#))
- [30] M. Lammers, Untersuchung der Untergrundrate des KATRIN Vorspektrometers im Bereich hoher Feldstärken, Diploma thesis, KIT, 2009. ([hyperlink](#))
- [31] S. Groh, Untersuchung von UV-Laser induziertem Untergrund am KATRIN Vorspektrometer, Diploma thesis, KIT, 2010. ([hyperlink](#))
- [32] F. Glück, Background theory: radial motion of electrons from spectrometer electrodes into the fluxtube, KATRIN internal report 2005, KATRIN BSCW 25-51. ([hyperlink](#))
- [33] J. A. Nelder and R. Mead, A Simplex Method for Function Minimization, *The Computer Journal* 7 (1965) 308. ([hyperlink](#))
- [34] W. H. Press et al., *Numerical Recipes in C* (Cambridge University Press, Cambridge, 2002).
- [35] S. Mertens et al., Background due to stored electrons following nuclear decays in the KATRIN

- spectrometers and its impact on the neutrino mass sensitivity, *Astropart. Phys.* 41 (2013) 52. ([hyperlink](#))
- [36] F. Glück, The axisymmetric aircoil system and the magnetic field in the main spectrometer, Talk at 10. KATRIN Collaboration Meeting, March 2006, Bad-Liebenzell. KATRIN BSCW,95/1/10. Session A2. ([hyperlink](#))
- [37] F. Glück et al., Air coil system and magnetic field sensor system, KATRIN internal report 2009, KATRIN BSCW 30-65-Design Report. ([hyperlink](#))
- [38] N. Wandkowsky, Design and Background Simulations for the KATRIN Main Spectrometer and Air Coil System, Diploma thesis, KIT, 2009. ([hyperlink](#))
- [39] S. Mertens, Study of Background Processes in the Electrostatic Spectrometers of the KATRIN experiment, PhD thesis, KIT, 2012 ([hyperlink](#))
- [40] F. Glück, N. Wandkowsky and T. Cristea-Platon, LFCS air coil current set computations by mathematical optimization, Talk at 23. KATRIN Collaboration Meeting, Oct. 2012, Karlsruhe, KIT. KATRIN BSCW 95/1/23 Session E2. ([hyperlink](#))
- [41] E. Otten, Removing trapped energetic electrons from the main spectrometer by dumping the central guiding field with a current pulse, KATRIN Internal Report, 2010. ([hyperlink](#))
- [42] D. Furse, Magnetic Pulse Measurements at the Monitor Spectrometer, Talk at 22. KATRIN Collaboration Meeting, March 2012, Karlsruhe, KIT. KATRIN BSCW 95-1-22, Session D1. ([hyperlink](#))
- [43] M. Fujita, The coil design of the superconducting MRI magnet, *IEEE Trans. Magn.* 24 (1988) 2907. ([hyperlink](#))
- [44] J. L. Kirschvink, Uniform Magnetic Fields and Double-Wrapped Coil Systems: Improved Techniques for the Design of Bioelectromagnetic Experiments, *Bioelectromagnetics* 13 (1992) 401. ([hyperlink](#))
- [45] I. Sasada, Y. Nakashima, Planar coil system consisting of three coil pairs for producing a uniform magnetic field, *J. Appl. Phys.* 99 (2006) 08D904. ([hyperlink](#))
- [46] J. W. Clark, A New Method for Obtaining a Uniform Magnetic Field, *Rev. Sci. Instrum.* 9 (1938) 320. ([hyperlink](#))
- [47] J. E. Everett, J. E. Osemeikhian, Spherical coils for uniform magnetic field, *J. Sci. Instrum.* 43 (1966) 470. ([hyperlink](#))
- [48] E. W. Cowan, *Basic Electromagnetism* (Academic Press, New York, 1968).
- [49] W. K. H. Panofsky and M. Phillips, *Classical Electricity and Magnetism* (Dover Publications, Mineola, New York, 1962).
- [50] W. R. Smythe, *Static and Dynamic Electricity* (McGraw Hill Book Company, 1968).
- [51] F. Glück, Earth-field compensation with cylindrical or ellipsoidal coil, Talk at KATRIN EMD Meeting, April 2004, Bonn; KATRIN BSCW 25-9-26-04-04. ([hyperlink](#))
- [52] A. Osipowicz, Compensation and manipulation of the magnetic field at the main spectrometer, KATRIN internal report 2005, KATRIN BSCW 25-1-earth magnetic field compensation. ([hyperlink](#))
- [53] F. Glück and A. Osipowicz, Air coil design at the main spectrometer, Talk at 14. KATRIN Collaboration Meeting, April 2008, Karlsruhe. KATRIN BSCW 95-1-14 Session D1. ([hyperlink](#))
- [54] The PartOpt project webpage <http://www.PartOpt.net/> ([hyperlink](#))
- [55] F. Glück, Axisymmetric magnetic field calculation with zonal harmonic expansion, *Progress In Electromagnetics Research B* 32 (2011) 351. ([hyperlink](#))
- [56] F. Glück, Axisymmetric electric and magnetic field calculations with zonal harmonic expansion, *PIERS Proceedings*, Kuala Lumpur, March 27-30, 2012, pages 1698-1702. ([hyperlink](#))
- [57] P. W. Hawkes and E. Kasper, *Principles of Electron Optics*, Vol 1 (Academic Press, Harcourt Brace Jovanovich, 1989).
- [58] T. J. Corona, Tools for Electromagnetic Field Simulation in the KATRIN Experiment, master thesis, MIT, 2009. ([hyperlink](#))
- [59] B. Leiber, Non-axially symmetric field and trajectory calculations for the KATRIN-experiment,

- Diploma thesis, KIT, 2010. ([hyperlink](#))
- [60] F. Glück, Axisymmetric Electric Field Calculation with Zonal Harmonic Expansion, Progress In Electromagnetics Research B 32 (2011) 319. ([hyperlink](#))
 - [61] M. Babutzka et al., The Comprehensive Guide to KASSIOPEIA, version 1.00.00 (KATRIN internal report). ([hyperlink](#))
 - [62] D. Furse et al., KASSIOPEIA – the simulation package for the KATRIN experiment (in preparation).
 - [63] J. Nocedal and S. J. Wright, Numerical Optimization (Springer, 2006).
 - [64] J. M. A. Bhatti, Practical Optimization Methods (Springer, New York, 2000).
 - [65] J. A. Snyman, Practical Mathematical Optimization (Springer, New York, 2005).